


# Photodynamic Cationic Ultrasmall Copper Oxide Nanoparticles-Loaded Liposomes for Alleviation of MRSA Biofilms

Xiangjun Chen\*, Wenting Li\*, Xueling Li, Keke Li , Guilong Zhang, Wei Hong

School of Pharmacy, Shandong New Drug Loading & Release Technology and Preparation Engineering Laboratory, Binzhou Medical University, Yantai, People's Republic of China

\*These authors contributed equally to this work

Correspondence: Wei Hong; Guilong Zhang, Tel/Fax +86-0535-6908191; Tel/Fax +86-0535- 6913719, Email hongwei\_sy@bzmc.edu.cn; glzhang@bzmc.edu.cn

**Introduction:** As we enter the post-antibiotic era, the rise of antibiotic-resistant pathogenic bacteria is becoming a serious threat to public health. This problem is further complicated by antibiotic-resistant biofilms, for which current treatment options are limited.

**Methods:** To tackle this challenge, we propose a novel approach that involves the use of photodynamic cationic pH-sensitive liposomes loaded with ultra-small copper oxide (Ce6@Lipo/UCONs) to effectively eliminate drug-resistant bacteria and eradicate biofilms while minimizing safety concerns and the risk of resistance development.

**Results:** Our study demonstrates that Ce6@Lipo/UCONs have minimal toxicity to mammalian cells and can significantly enhance the association affinity with methicillin-resistant *Staphylococcus aureus* (MRSA) as confirmed by fluorescent microscope and flow cytometry, thereby greatly improving the bactericidal effect against planktonic MRSA. The cationic nature of Ce6@Lipo/UCONs also enables them to penetrate MRSA biofilms and respond to the acidic microenvironment within the biofilm, effectively releasing the loaded UCONs. Our results indicate that Ce6@Lipo/UCONs could effectively eliminate biofilms under light irradiation conditions, as evidenced by both biomass analysis and scanning electron microscopy observations. In addition, significant antibacterial effects and abscess healing were observed in MRSA-infected mice treated with Ce6@Lipo/UCONs upon light irradiation, while good biocompatibility was achieved in vivo.

**Conclusion:** Taken together, our findings suggest that photodynamic cationic ultrasmall copper oxide nanoparticles-loaded liposomes are a highly promising nano platform for combating antibiotic-resistant microbial pathogens and biofilms. The effective biofilm penetration and synergistic effect between photodynamic inactivation and metal sterilization make them a valuable tool for overcoming the challenges posed by antibiotic resistance.

**Keywords:** biofilm, antibiotic resistance, synergistic potential, photodynamic inactivation, metal sterilization

## Introduction

The use of antibiotics has greatly reduced the threat of bacterial infections.<sup>1-4</sup> However, overuse and misuse of antibiotics have led to the emergence of antimicrobial resistance (AMR). As one of the most well-known multidrug-resistant (MDR) bacteria, gram-positive methicillin-resistant *Staphylococcus aureus* (MRSA) can cause various infections such as sepsis, pneumonic, and endocarditis. Over the years, MRSA has developed resistance to multiple antibiotics, including vancomycin.<sup>5-7</sup> Biofilms, formed by bacteria that aggregate together within a matrix of extracellular polymeric substances (EPS), create a formidable barrier to effective anti-bacterial treatments and evade the host immune system.<sup>8,9</sup> MRSA is capable of forming biofilms, which enable it to persist in clinical settings for extended periods of time. Since conventional antibiotics are ineffective against resistant bacteria and biofilms, there is an urgent need to develop alternative antibacterial approaches.<sup>10-12</sup>

Photodynamic therapy (PDT) is a promising approach for combating drug-resistant bacteria due to its minimal trauma and low toxicity.<sup>13–16</sup> Unlike conventional antibiotic therapies, the mechanism of action of antibacterial PDT is less likely to lead to the development of resistance. However, because of the barrier formed by biofilms, penetration and accumulation of photosensitizers (PS), like many other drugs, are greatly limited, and thus PDT has not reached its potential in removing biofilms. To address this issue, PS-loaded nanocarriers have been developed to not only increase the aqueous solubility of PS but also improve the targeted delivery of PS at the infected sites. Surface charge and size are two main factors to consider during the designing of new nanocarriers. The bacterial membranes are negatively charged, which can be selectively targeted when the nanocarriers are positively charged.<sup>17–20</sup> In addition, small nanoparticles (NPs) demonstrate a superior ability to infiltrate and remain in biofilms, because small NPs experience less diffusional hindrance. Studies have shown that the diameter of an efficient NP should be smaller than 3 nm, which can achieve almost 75% penetration of biofilms.<sup>21–25</sup>

Metal ions, such as silver and copper, have been widely used to treat infection and prevent bacterial contamination before the development of antibiotics.<sup>19,26–28</sup> These metal materials are advantageous not only because of their antibacterial abilities but also because of the low likelihood of resistance.<sup>29</sup> Among the metal oxides, ultra-small copper oxide nanoparticles (UCONs) have gained significant attention in recent years.<sup>26</sup> Firstly, unlike gold, platinum, and silver, copper is a trace element necessary for the human body and may have good biocompatibility.<sup>19,26,27</sup> Second, the cost of acquiring copper oxide is relatively low. Third, the ultra-small size of the particles may overcome the barrier of biofilms, leading to the penetration and specific targeting of pathogens. However, it is important to note that applications of a significant amount of heavy metals should be cautious in practical use.

Various drug delivery systems have been developed, which could efficiently deliver encapsulated drugs to their targets. Among these carriers, liposomes have attracted numerous attentions due to the efficacious interaction with cells, extended plasma half-life, enhanced accumulation and retention at the site of infection, and reduced cellular toxicity.<sup>30</sup> Up to now, liposomes have been successfully developed for commercially available antibiotics, such as mupirocin, aminoglycosides and polymyxin.<sup>31–33</sup> It is well demonstrated that the encapsulation of EPS creates an oxygen-deficient biofilm microenvironment, which can lead to anaerobic glycolysis. As a result, acidic and highly reducing conditions are prevalent in many biofilms. As an example, the pH within MRSA biofilm microenvironments may decrease to 5.5 or even below, while the GSH concentrations in *E. coli* biofilms can be as high as 10 mM.<sup>34,35</sup> Thus, exploiting the distinctive biofilm microenvironment necessitates the creation of novel approaches to address biofilm infections, especially those caused by bacteria resistant to multiple drugs.

In this study, to address the issue of antibiotic resistance in MRSA biofilms, we developed photodynamic cationic pH-sensitive liposomes loaded with ultra-small copper oxide (denoted as Ce6@Lipo/UCONs). We expect that this construct will have the following advantages: 1) The positively charged Ce6@Lipo/UCONs can penetrate into the biofilm through electrostatic interaction with MRSA, 2) The pH-sensitive phospholipids will promptly protonate to release UCONs for complete biofilm penetration after initial penetration, and 3) Bacteria killing and biofilm ablation can be achieved through a synergistic effect between photodynamic inactivation and metal sterilization. (Scheme 1).

## Materials and Methods

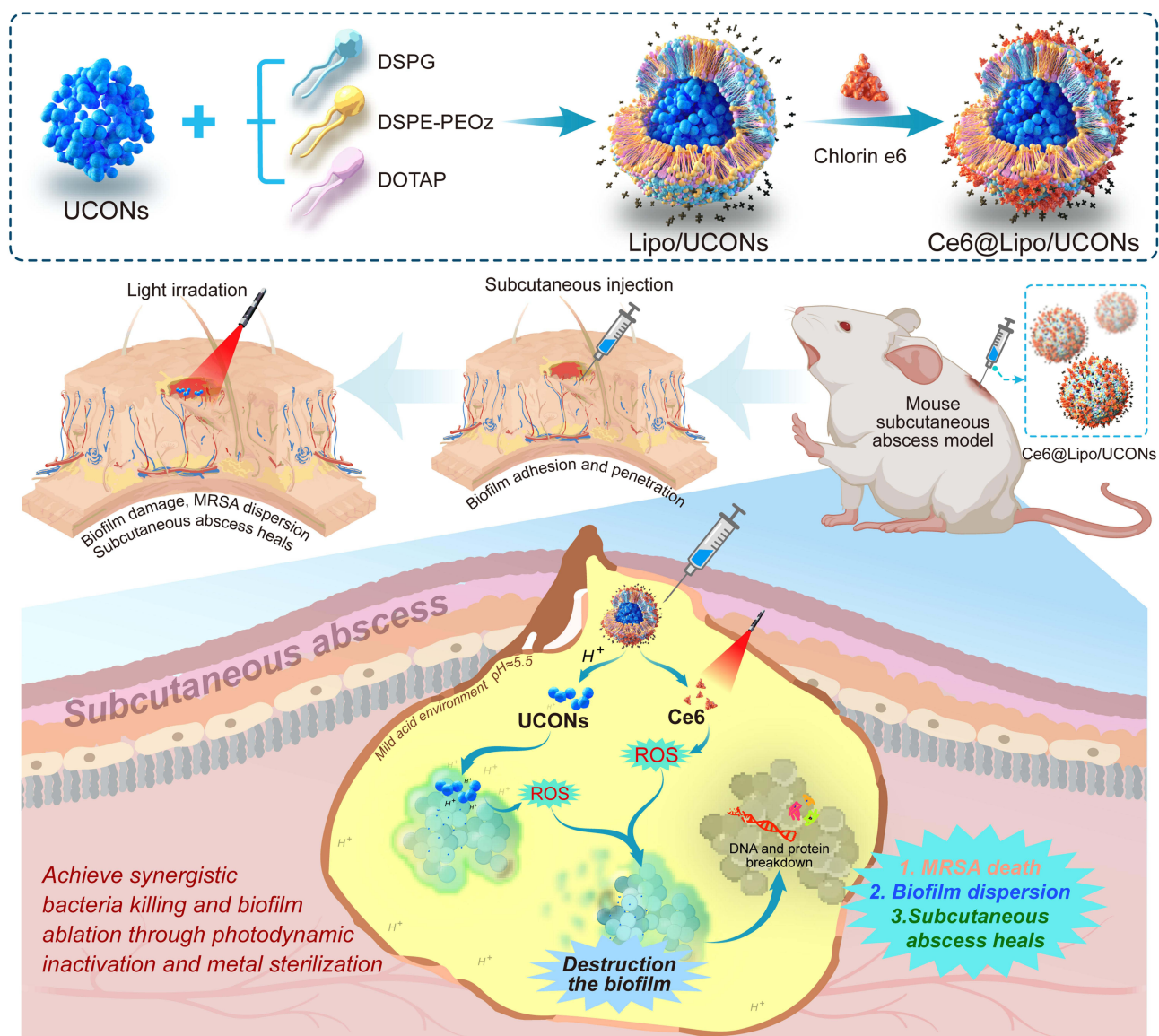
### Materials

The materials used in this study are listed in the Electronic [Supplementary Information](#).

### Methods

#### Preparation and Characterization of UCONs and Ce6@Lipo/UCONs

Ultrasmall copper oxide nanoparticles (UCONs) were synthesized via a facile modified method. Briefly, the CuCl<sub>2</sub> solution (0.2 M, 10 mL) was added into three-necked and round-bottomed flask, and stirred for 10 min at 80 °C using an oil bath. Next, L-ascorbic acid aqueous solution (0.5 M, 50 mL) was added dropwise into the flask along with vigorous stirring. The resulting solution was continuously stirred at 80 °C for 24 h and the color changed from blue to form dark brown solution. Subsequently, the aggregated particles were removed by centrifugation (6000 rpm/min, 10 min).



**Scheme 1** Schematic illustration of photodynamic cationic ultrasmall copper oxide nanoparticles-loaded liposomes (Ce6@Lipo/UCONs) for alleviation of MRSA Biofilms.

Meanwhile, the supernatant was purified using a dialyzed method to remove small molecules and other impurities. Finally, UCONs were washed using the distilled water, and then collected by centrifugation. The morphologies of UCONs were observed on a transmission electron microscope (TEM, JEM-1400, JEOL, Japan). The structure and interaction were analyzed using a Fourier transform infrared (FTIR) spectrometer (Nicolet IS10, Co., America). Zeta potential and particle size distribution of UCONs in distilled water was determined by a dynamic light scattering detector (ZS90, Malvern, UK).

Ce6@Lipo/UCONs was prepared by two steps. In the first step, Lipo/UCONs were produced by the ethanol injection method. A mixture of DSPG (50.0 mg), DOTAP (20.0 mg), DSPE-PEO<sub>z</sub> (15.0 mg) and Chol (10.0 mg) was added into 5.0 mL of UCONs ethanol solution (0.5 mg/mL) under sonication for 15 min. Then, the mixture was slowly added to 10 mL PBS (pH 7.4) at 50 °C, and the ethanol was removed from the mixture by rotary evaporation. The Lipo/UCONs were obtained after the unincorporated UCONs were removed by filtration through a 0.22 μm film. In the second step, to load Ce6 onto the Lipo/UCONs, 150 μL of Ce6 dissolved in sulfoxide (2 mg/mL) was added to 10 mL of Lipo/UCONs mixture, and the resulting solution was stirred for 2 h, followed by filtration to remove any unbound Ce6. The purified Ce6@Lipo/UCONs were stored at 4 °C for future use.

The physiochemical properties of Lipo/UCONs and Ce6@Lipo/UCONs, such as morphology, zeta potential and particle size, were evaluated, and entrapment efficiency (EE%) and drug loading (DL%) of UCONs were calculated using (Equations 1 and 2), respectively:

$$EE\% = \frac{\text{Weight of UCONs in liposomes}}{\text{Weight of the feeding UCONs}} \times 100\% \quad (1)$$

$$DL\% = \frac{\text{Weight of UCONs in liposomes}}{\text{Weight of the freezed Ce6@Lipo/UCONs}} \times 100\% \quad (2)$$

Where, the weight of UCONs was calculated from the concentration of  $\text{Cu}^{2+}$ , which was measured using an Inductively Coupled Plasma-Optical Emission Spectrometry (PerkinElmer Avio<sup>®</sup>220 Max), and the Ce6 content in Ce6@Lipo/UCONs was calculated by measuring the absorbance at 660 nm.

The release behavior of UCONs from liposomal UCONs was evaluated at two different pH (5.5 and 7.4). The experiment involved placing 2 mL of Lipo/UCONs and Ce6@Lipo/UCONs in a dialysis bag (with a molecular weight cut-off of 100 kDa) containing 20 mL of pH 5.5 and pH 7.4 PBS, respectively. A total of 400  $\mu\text{L}$  of the dialysis solution was sampled at specific time intervals to determine the concentration of  $\text{Cu}^{2+}$  by ICP-OES.

To determine the level of ROS generated in vitro, the probe 2,7-dichlorofluorescein diacetate (DCFH-DA) was employed. According to a previously reported procedure, dichlorofluorescein (DCFH) was prepared by incubating 3  $\mu\text{L}$  DCFH-DA (2.5 mM) with 150  $\mu\text{L}$  NaOH (0.01 mol/L) for 30 min, followed by reaction termination by adding 150  $\mu\text{L}$  PBS. Subsequently, 100  $\mu\text{L}$  DCFH was mixed with 300  $\mu\text{L}$  of PBS, Ce6, UCONs, Lipo/UCONs and Ce6@Lipo/UCONs, respectively. After irradiation (100  $\text{mW}/\text{cm}^2$ , 10 min), the change of fluorescence intensity was evaluated using 488 nm as the excitation wavelength, and the emission spectra were recorded from 500 nm to 600 nm.

### In vitro Biocompatibility Analysis

Cell viability test and hemolysis assay were conducted to evaluate the in vitro biocompatibility of UCONs, Lipo/UCONs, and Ce6@Lipo/UCONs, and determined as described in our previous report.<sup>36</sup> The cytotoxicity of the tested formulations was evaluated against Vero cells. Vero cells were purchased from American Type Culture Collection (Manassas, VA, USA), and cultured in DMEM media (Gibco BRL, Grand Island, NY) containing 10% FBS. The cell viabilities were measured by an CCK-8 assay after being incubated with different formulations with a UCONs concentration ranging from 8 to 128  $\mu\text{g}/\text{mL}$  overnight. For hemolysis assay, the concentration of UCONs also ranged from 8 to 128  $\mu\text{g}/\text{mL}$ , and calculated by (Equation 3):

$$\text{Hemolysis (\%)} = \frac{[(OD_t - OD_0) / (OD_{100} - OD_0)] \times 100\%}{\quad} \quad (3)$$

where,  $OD_t$  is the optical density of the cells treated with UCONs, Lipo/UCONs, and Ce6@Lipo/UCONs at the concentration of t, and  $OD_0$  and  $OD_{100}$  are the optical density treated with saline and 0.5% Triton X-100, respectively.

### Bacterial Binding Affinity and Biofilm Penetration

#### Bacterial Binding Affinity

Free Ce6 and Ce6@Lipo/UCONs were added to MRSA suspensions at pH 7.4 and pH 5.5, respectively, and incubated for 2 h. A small portion of the MRSA suspensions (1 mL) was collected from each suspension, centrifuged, and resuspended in 100  $\mu\text{L}$  of pH 7.4 PBS. The fluorescence images of the bacteria were captured using a fluorescent microscope (Olympus BX53F2, Japan). In addition, a BD FACSCanto II flow cytometry (USA) was employed to measure the fluorescence of the pretreated bacteria, while the untreated bacteria served as the negative control.

#### Biofilm Penetration

The biofilms used in this study were fabricated as previously described,<sup>36</sup> which were incubated with free Ce6 or Ce6@Lipo/UCONs at different pH (7.4 and 5.5) for 1 h, respectively. Green fluorescent imaging of the biofilms was performed after staining with SYTO 9 dye for 30 min using a confocal laser scanning microscopy (Zeiss LSM 880, Germany). An interval of 1  $\mu\text{m}$  was used for the Z-stack images.



## In vitro Antibacterial Experiments

### MICs Determination

To determine the antibacterial activities of UCONs, Lipo/UCONs, and Ce6@Lipo/UCONs, the minimal inhibitory concentrations (MICs) against MRSA USA300 were measured through a micro-dilution method at pH 7.4 and 5.5. The NIR power density was set as 100 mW/cm<sup>2</sup>, and the irradiation time was set as 10 min.

### Bacterial Fluorescent Imaging

The toxicity of UCONs, Lipo/UCONs, and Ce6@Lipo/UCONs against bacteria was assessed using a Live/Dead BacLight bacterial viability kit. First, the cells were treated with 8 µg/mL of the UCONs or UCONs-loaded liposomes overnight at pH 7.4, 5.5, and 5.5+NIR, respectively, with a power density of 100 mW/cm<sup>2</sup> and an irradiation time of 10 min. Second, after being washed with PBS, the bacterial cells were stained with SYTO 9 and PI dyes for 30 min at 37°C in the dark. The stained bacterial cells were then observed using an optical microscope. (BX53F2 Optical Microscope, Japan).

### Morphology of Bacteria

The bacterial cells were firstly treated with 8 µg/mL of UCONs, Lipo/UCONs, and Ce6@Lipo/UCONs at pH 5.5 with irradiation at 100 mW/cm<sup>2</sup> for 10 min. Then, the bacterial cells were collected by centrifuge at 3600 rpm for 5 min. To prepare the samples for morphological observation, the bacterial cells were fixed with 2.5% glutaraldehyde at 25°C for 2 h and treated with ethanol. The dehydrated bacterial cells were then placed on a silica wafer and visualized using a scanning electron microscope (Zeiss EVO LS15, Germany).

### In situ Detection of ROS Production

The production of reactive oxygen species (ROS) in bacterial cells was assessed after being incubated with different formulations (PBS, free Ce6, UCONs, Lipo/UCONs, and Ce6@Lipo/UCONs) at pH 7.4, 5.5, or 5.5+NIR (100 mW/cm<sup>2</sup>, 10 min) at 37°C for 2 h. The bacterial cells were washed with PBS and treated with DCFH-DA at a final concentration of 10 µM for 30 min at 37°C. After centrifugation and washing with PBS three times, fluorescent images of the bacterial cells were recorded using a fluorescent microscope (Olympus BX53F2, Japan).

### Biofilm Eradication Assay

#### Biofilm Eradication and Quantification

To evaluate the biofilm eradication efficacy of different formulations (PBS, free Ce6, UCONs, Lipo/UCONs, and Ce6@Lipo/UCONs,) mature biofilms were incubated with these agents for 12 h and then the biofilm biomass was quantified using the crystal violet (CV) method. The irradiation time was set at 10 minutes, with a power density of NIR at 100 mW/cm<sup>2</sup>. In these formulations, the concentrations of UCONs and free Ce6 were set at 32.0 µg/mL and 4.0 µg/mL, respectively. The biofilms were stained with a 0.5% (w/v) CV solution for 10 min, and then 200 µL 95% ethanol (v/v) was added to replace the CV solution, after which the biofilm biomass was quantified by measuring the absorbance at 590 nm on a microplate reader (BioTek Synergy H1, USA).

#### SEM Imaging of the Biofilms

The biofilms treated with different formulations (PBS, free Ce6, UCONs, Lipo/UCONs, and Ce6@Lipo/UCONs) were subjected to SEM analysis to determine their morphology. Mature biofilms that had grown for 96 h were exposed to these formulations with UCONs and free Ce6 concentrations of 32 µg/mL and 4.0 µg/mL, respectively, for 12 h in 24-well plates. The biofilms were then fixed, gradually dehydrated, and coated with gold before being observed on a SEM (Zeiss EVO LS15, Germany). The power density of NIR was set at 100 mW/cm<sup>2</sup>, and the irradiation time was 10 min.

#### ROS Production in Biofilms

To investigate ROS production in MRSA biofilms, the ROS indicator DCFH-DA was used to stain the biofilms treated with different formulations (PBS, free Ce6, UCONs, Lipo/UCONs, and Ce6@Lipo/UCONs with or without NIR) for 2

h. The fluorescence of the biofilm was recorded using a confocal laser scanning microscopy (Zeiss LSM 880, Germany). An interval of 1  $\mu\text{m}$  was used for the Z-stack images.

### In vivo Anti-Biofilm Efficiency

Back abscess-bearing mice were used in this study, which were administered subcutaneously with 50  $\mu\text{L}$  MRSA USA300 and then randomly divided into five groups. On the day 4 after infection, the mice were subcutaneously injected with 200  $\mu\text{L}$  of different formulations: (i) saline, (ii) free Ce6, (iii) UCONs, (iv) Lipo/UCONs, or (v) Ce6@Lipo/UCONs at a dose of 2 mg/kg UCONs, respectively. After the treatment, the abscess was irradiated with 660 nm light (100 mW/cm<sup>2</sup>) for 10 min. And then after 48 h, a second treatment with the same dose was applied. The body weight of the mice was monitored daily. H&E staining and Gram's staining were used to analyze the MRSA-infected tissues after the treatment on day 9. The bacterial load was determined after the abscesses were homogenized. Additionally, main organs, including the kidney, lung, liver, heart, and spleen, were collected and evaluated for in vivo toxicity using H&E staining.

### Statistical Analyses

Statistical analyses were performed using Student's *t*-test, and the data were reported as mean  $\pm$  standard deviation (S.D). The significance level was represented as \**P* <0.05, \*\**P* <0.01, \*\*\**P* <0.001, and \*\*\*\**P* <0.0001 for the respective levels of statistical significance.

## Results and Discussions

### Characterization of UCONs and UCONs-Loaded Liposomes

UCONs were successfully synthesized using cupric chloride and L-ascorbic acid as reaction precursor. TEM images showed that UCONs were uniform and their size was only approximate  $\sim 3$  nm (Figure 1a). HRTEM image of UCONs cannot observe significant fringer lattice, indicating that UCONs might be amorphous (Figure 1b). In addition, Ce6@Lipo/UCONs were fabricated by the direct encapsulation of Ce6 molecules and UCONs using liposome. Figure 1c indicated that Ce6@Lipo/UCONs were significantly larger than that of UCONs and presented cluster-like nanostructure. X-ray diffraction (XRD) analysis of Ce6@Lipo/UCONs did not show significantly diffraction peaks, and only had a wide peak at the range of 10–30° degree, further confirming the amorphous state (Figure 1d). Subsequently, the composition of Ce6@Lipo/UCONs was analyzed using XPS spectra. As shown in Figure 1e, XPS full spectra of Ce6@Lipo/UCONs demonstrated the presence of C, N, O, and Cu elements. Moreover, Cu2p peaks appeared at 932.1 and 952.3 eV (Figure 1f), corresponding to Cu(I) in the paramagnetic chemical state, indicating that UCONs should be Cu<sub>2</sub>O ultrasmall nanoparticles. Besides, C1s spectra showed three peaks at 284.5, 285.9, and 288.2 eV, which were respectively assigned to C-C, C=C, and C=O (Figure 1g), confirmed the successful encapsulation Ce6 molecules and liposomes. The composition of Ce6@Lipo/UCONs was also further analyzed using FT-IR. It could be seen in Figure 1h that Ce6@Lipo/UCONs showed significant peaks of -P=O and -C=C bonds, further demonstrating the successful fabrication of Ce6@Lipo/UCONs. DLS analysis showed that the hydrodynamic size of UCONs only about  $9.26 \pm 1.15$  nm, however, Lipo/UCONs increased to  $82.58 \pm 0.80$  nm. Notably, compared to Lipo/UCONs, the hydrodynamic size of Ce6@Lipo/UCONs had no significant variation, implying that the loading of photosensitizer Ce6 cannot affect the colloidal stability of particles (Figure 1i). Further loading Ce6 onto the Lipo/UCONs led to a decrease in both zeta potential to  $+37.73 \pm 3.71$  mV, due to the neutralization of charges. The average drug loading content of Ce6 and UCONs were 0.281 and 2.25%, respectively. The encapsulation efficiency of UCONs was above 85%.

For outstanding antibacterial activity, an efficient drug release controlled by stimuli should be important. The release profile of UCONs from Ce6@Lipo/UCONs was evaluated at different pH conditions. As illustrated in Figure 1j, the cumulative release of UCONs from Ce6@Lipo/UCONs exhibited a sustained release profile at physiological conditions (pH 7.4); less than 25% of UCONs were released over an 8-hour period. This finding suggests that liposomes maintain their structural stability at physiological pH and effectively restrict the release of UCONs. However, when the pH was adjusted to mimic the acidic biofilm microenvironment (pH 5.5), a rapid release of UCONs was observed. Over a 4-hour period, nearly 60% of UCONs were released and over 90% were released after 24 hours. The remarkable contrast in the release pattern of UCONs observed at varying pH values confirms the pH-sensitive nature of the system and the

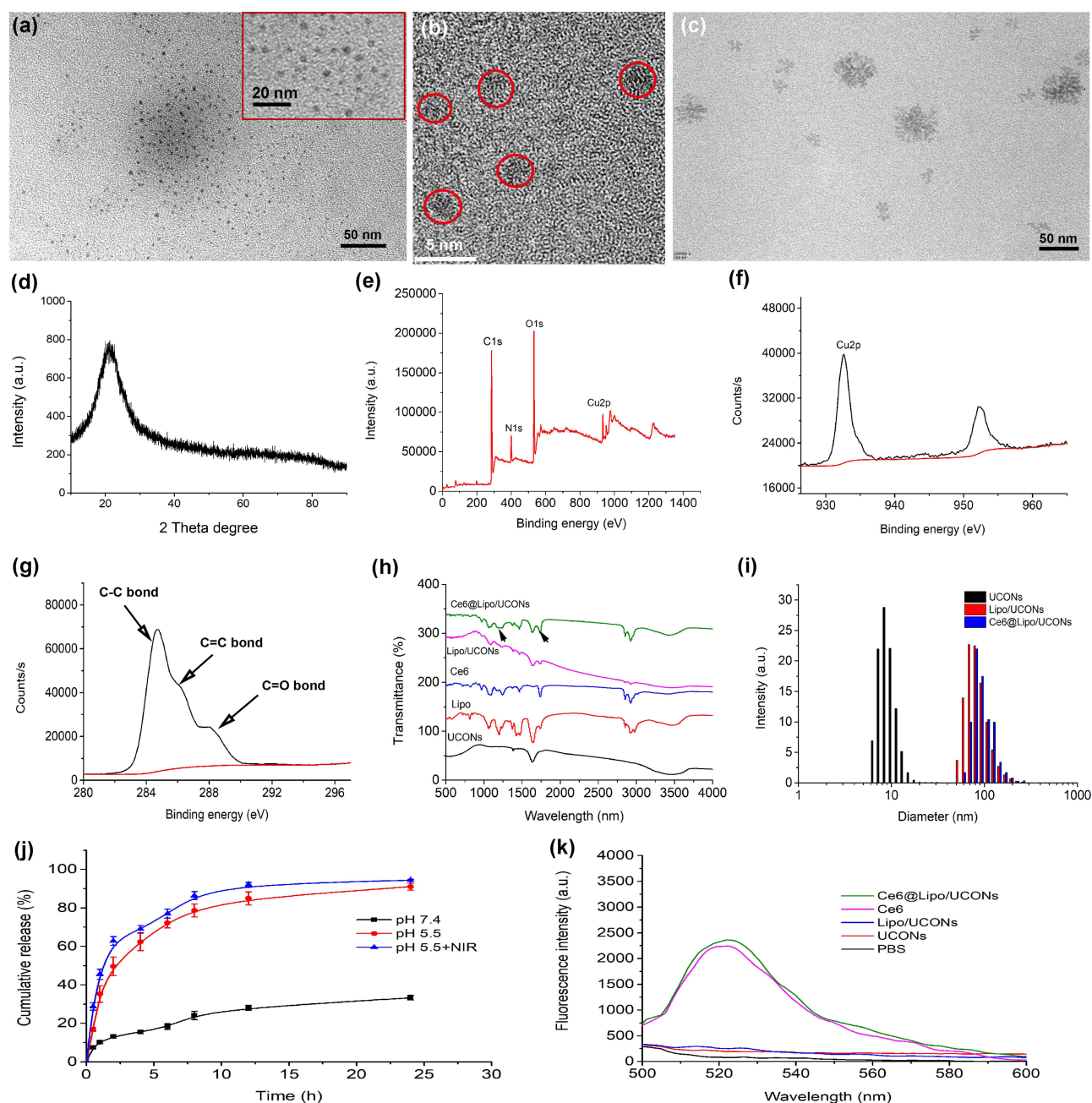


**Figure 1** (a) TEM image and (b) high-resolution TEM image of UCONs; (c) TEM image of Ce6@Lipo/UCONs; (d) XRD spectra of Ce6@Lipo/UCONs; (e) XPS full spectra, (f) Cu2p spectra, and (g) C1s spectra of Ce6@Lipo/UCONs; (h) FT-IR spectra of Ce6@Lipo/UCONs; (i) hydrodynamic size of UCONs, Lipo/UCONs, and Ce6@Lipo/UCONs. (j) Cumulative release of UCONs from Ce6@Lipo/UCONs by different treatments (pH 5.5, pH 7.4 and pH 5.5+NIR). (k) Plots of the absorbance change of DCFH after incubation with different formulations (PBS, UCONs, Lipo/UCONs, Ce6 and Ce6@Lipo/UCONs) under irradiation.

destabilization of liposomal structure in acidic environments. It is worth noting that irradiation also accelerated the release of UCONs. Upon irradiation, an initial burst release of up to 28% was obtained within 0.5 h, which could be attributed to the increased fluidity of the phospholipid bilayer caused by the photothermal effect of Ce6.

To evaluate the production of ROS, the fluorescent probe DCFH-DA was utilized, which emits green fluorescence in the presence of ROS. As depicted in Figure 1k, the fluorescence intensities of PBS, UCONs, and Lipo/UCONs remained almost constant, indicating that Lipo/UCONs themselves do not have a photosensitizing effect. Conversely, Ce6@Lipo/UCONs produced a considerable amount of ROS when exposed to a 660 nm laser, similar to that of free Ce6. These findings indicate that the presence of Ce6 on Lipo/UCONs does not hinder the photosensitizing ability of Ce6.

## Hemolysis and Cytotoxicity Behavior

Evaluation of the biocompatibility of nanoparticles is crucial to determine their potential for biomedical applications. In this study, the impact of UCONs, Lipo/UCONs, and Ce6@Lipo/UCONs on the viability of Vero cells were assessed *in vitro* (Figure 2a). The results show that these nanoparticles did not exhibit significant toxicity towards the cells even at a concentration as high as 128  $\mu\text{g}/\text{mL}$  (equivalent to UCONs), as the survival rate remained above 90%. Additionally, undesirable effects to the host tissues, such as erythrocyte lysis, were measured to assess the biocompatibility of these nanoparticles. The results demonstrated that the hemolysis rate (<5%) caused Ce6@Lipo/UCONs was negligible in blood cells, even at concentrations as high as 64  $\mu\text{g}/\text{mL}$  (Figure 2b). These results indicate that the *in vitro* safety of Ce6@Lipo/UCONs is acceptable, expanding the possibilities for its use in future applications.

## Bacterial Binding Affinity and Biofilm Penetration Behavior

To measure the binding ability of liposomes with bacteria, we utilized fluorescence microscopy and flow cytometry to observe the MRSA cells after treatments with free Ce6 and Ce6@Lipo/UCONs. The results depicted in Figure 3a indicated that free Ce6 could only be weakly absorbed by MRSA, as indicated by the faint red fluorescence. In contrast, the cells treated with Ce6@Lipo/UCONs exhibited strong red fluorescence, indicating their enhanced binding ability with MRSA. Similar results were observed by flow cytometry, as depicted in Figure 3b. Moreover, it is noteworthy that the fluorescent intensity of Ce6@Lipo/UCONs at pH 5.5 was lower compared with that of pH 7.4, which may be attributed to the disassociation of Ce6@Lipo/UCONs under the acidic condition. However, even at pH 5.5, the fluorescent intensity was higher than that of Ce6, indicating that the binding affinity was still increased under this condition. Thus, the enhanced binding affinity of Ce6@Lipo/UCONs could potentially advance the delivery of both Ce6 and UCONs.

Biofilms form a strong barrier, which greatly hinders the delivery of common anti-bacterial agents. To assess the penetration ability of Ce6@Lipo/UCONs, 3D CLSM was employed. As shown in Figure 3c, when the biofilm was treated with free Ce6, no obvious red fluorescence was detectable within the biofilm. However, when the biofilm was treated with Ce6@Lipo/UCONs, the intensity of red fluorescence was greatly enhanced, indicating Ce6@Lipo/UCONs exhibit excellent penetration and diffusion ability into MRSA biofilms at both pHs. The positively charged Ce6@Lipo/UCONs could be advantageous in promoting improved penetration and accumulation in biofilms. Additionally, the penetration behavior of Ce6@Lipo/UCONs was not affected by pH values, indicating that Ce6 could be effectively delivered into biofilms before dissociation.

## In vitro Antibacterial Activity

The antibacterial activities of UNCONs, Lipo/UCONs and Ce6@Lipo/UCONs were firstly evaluated under different pHs. As illustrated in Table 1, both Lipo/UCONs and Ce6@Lipo/UCONs showed pH-dependent antibacterial activity. At pH 7.4, both Lipo/UCONs and Ce6@Lipo/UCONs had a MIC value of 512  $\mu\text{g}/\text{mL}$ , but this value decreased significantly to 32  $\mu\text{g}/\text{mL}$  at pH 5.5, which is equivalent to that of UCONs. The enhanced antibacterial potency was attributed to the efficient release of UCONs. Moreover, the photodynamic antibacterial efficacy of Ce6@Lipo/UCONs was further

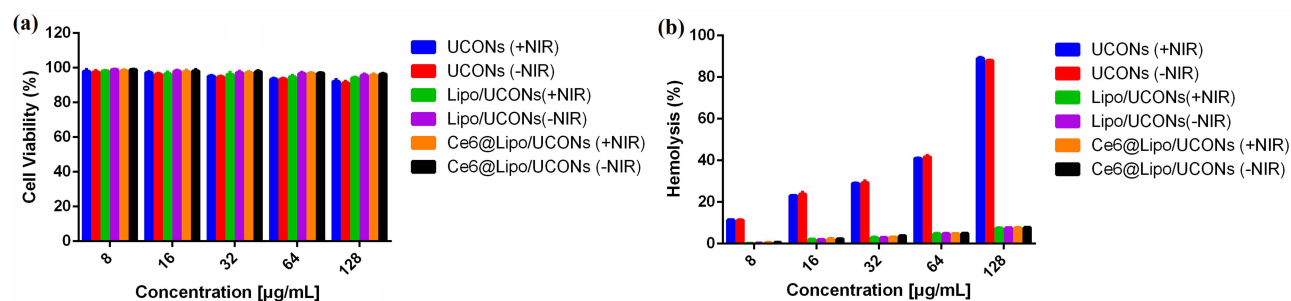
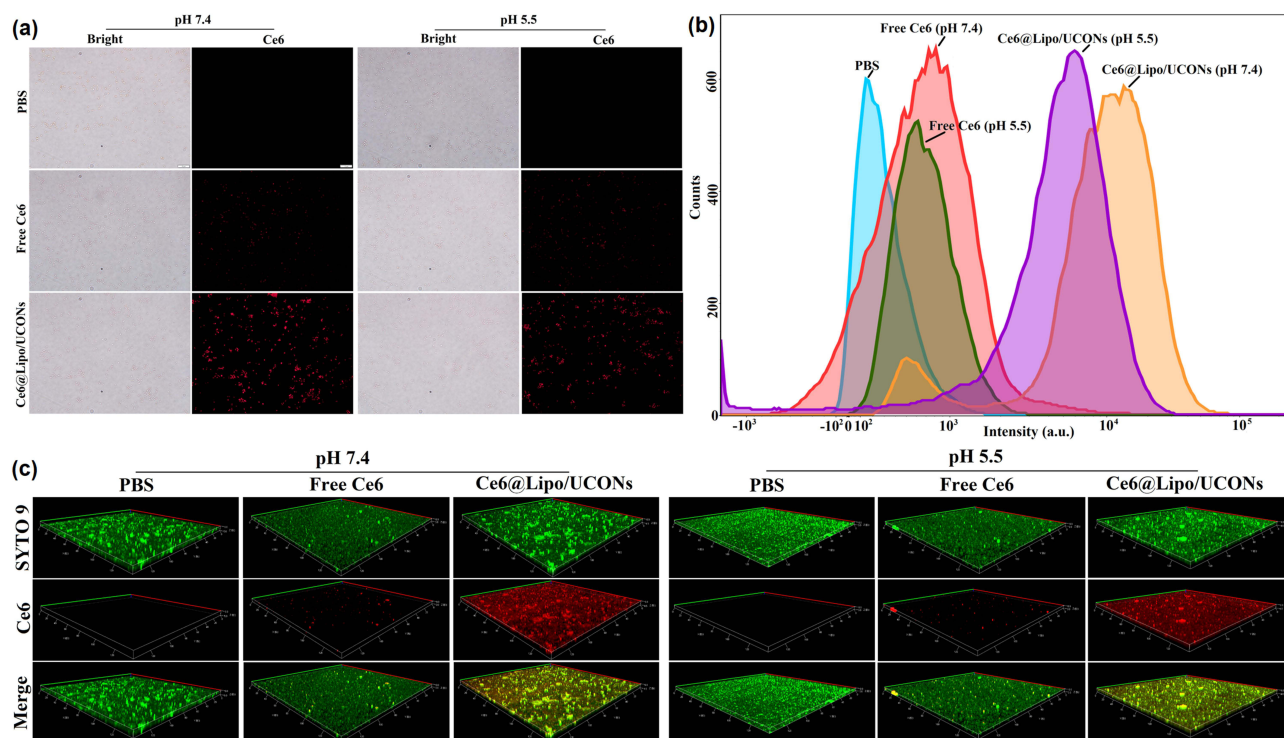


Figure 2 (a) Cell cytotoxicity evaluation and (b) hemolysis analysis of UCONs, Lipo/UCONs and Ce6@Lipo/UCONs.





**Figure 3** Enhanced bacteria association of Ce6@Lipo/UCONs. (a) Fluorescence microscope observation and (b) flow cytometry analysis of MRSA suspensions treated with different formulations (free Ce6 and Ce6@Lipo/UCONs) at pH 7.4 and 5.5, respectively. (c) 3D CLSM images of MRSA biofilms treated with different formulations (PBS, free Ce6 and Ce6@Lipo/UCONs) at different pHs (7.4 and 5.5).

assessed. After irradiation, the MIC value of Ce6@Lipo/UCONs decreased to 8.0  $\mu\text{g/mL}$ . At this concentration alone, neither free Ce6 (approximately 1.0  $\mu\text{g/mL}$ ) nor UCONs (8.0  $\mu\text{g/mL}$ ) demonstrated any antibacterial activity.

The antibacterial effect of Ce6@Lipo/UCONs on planktonic bacteria cells was further investigated using a Live/Dead assay. The concentrations of Ce6 and UCONs were set as 1.0  $\mu\text{g/mL}$  and 8.0  $\mu\text{g/mL}$ , respectively. The results show that free Ce6, Lipo/UCONs and Ce6@Lipo/UCONs alone exhibited limited bactericidal activity at pH 7.4 (Figure 4a). Although the antibacterial effect of free Ce6 was improved under light irradiation, most of the bacteria cells were still alive. The antimicrobial efficacy of Lipo/UCONs and Ce6@Lipo/UCONs was enhanced upon exposure to an acidic environment at pH 5.5, owing to the effective release of UCONs. Notably, the combination of metal sterilization and photodynamic inactivation exhibited by Ce6@Lipo/UCONs resulted in complete eradication of MRSA under pH 5.5+NIR.

SEM images of MRSA were compared to investigate the changes of bacterial morphologies under different treatments (Figure 4b). In the blank control group, all microbes retained their characteristic shapes and smooth surfaces. No obvious disruption was observed on the surface of the bacteria cells treated with UCONs, and only a few displayed irregular shapes. When the MRSA cells were treated with Ce6@Lipo/UCONs under pH 5.5+NIR,

**Table 1** MIC Values of UNCONs and UCONs-Loaded Liposomes Against MRSA USA300

| Formulations   | MIC ( $\mu\text{g/mL}$ ) |        |            |
|----------------|--------------------------|--------|------------|
|                | pH 7.4                   | pH 5.5 | pH 5.5+NIR |
| UNCONs         | 32                       | 32     | 32         |
| Lipo/UCONs     | 512                      | 32     | 32         |
| Ce6@Lipo/UCONs | 512                      | 32     | 8          |

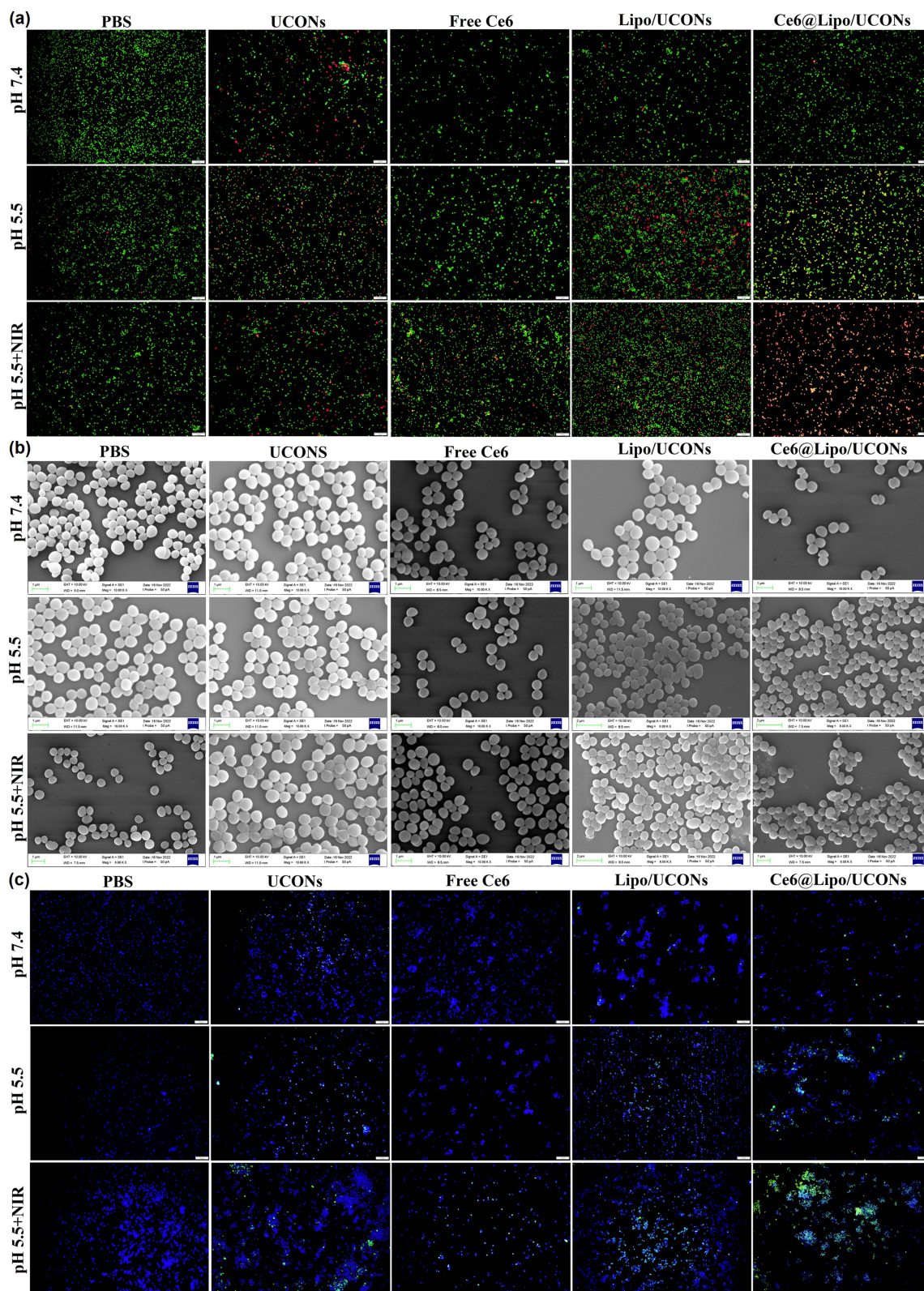


**Figure 4** (a) Live/Dead assay, (b) SEM images and (c) ROS generation of MRSA treated with different formulations (PBS, free Ce6, UCONs, Lipo/UCONs and Ce6@Lipo/UCONs under pH 7.4 and 5.5).

microbial deformations and wrinkled surfaces were observed. In contrast, these changes were not observed when treated with free Ce6+NIR.

The primary antibacterial mechanism of Ce6@Lipo/UCONs is believed to be oxidative stress damage. A large amount of reactive oxygen species (ROS) can be produced when Ce6 and UCONs are present, which can oxidize biomolecules of bacteria such as DNA, proteins, and lipids, ultimately resulting in death of bacterial cells. Thus, we investigated the ROS generation capability of Ce6@Lipo/UCONs upon light irradiation using DCFH-DA dye as an indicator (green fluorescence). Figure 4c demonstrates that UCONs were able to regulate the ROS production, with noticeable green fluorescence observed in MRSA following the treatment. As anticipated, the MRSA treated with Ce6@Lipo/UCONs under light irradiation exhibited the strongest green fluorescence, indicating the highest potential for producing ROS and antibacterial activity. Additionally, the fluorescent signals of MRSA overlapped with ROS production, demonstrating that Ce6@Lipo/UCONs induced an in situ ROS production in the bacteria cells. These results demonstrate that a synergistic bactericidal effect of Ce6@Lipo/UCONs could be realized by combining metal sterilization and photodynamic inactivation against MRSA.

## Ablation of Bacterial Biofilms

Taking advantage of the effective biofilm penetration of Ce6@Lipo/UCONs, we assessed their performance in biofilm ablation using crystal violet staining and SEM observation. The free Ce6 treatment, with or without irradiation, did not significantly alter the biofilm structure. Similarly, treatment with UCONs or Lipo/UCONs at the tested concentration (32 µg/mL) only showed weak dispersal efficacy on the biofilms. In contrast, under irradiation, the biofilm treated with Ce6@Lipo/UCONs was noticeably lighter compared with that without light irradiation (Figure 5a). The changes of biofilm remaining after the treatments were shown in Figure 5b. Without NIR, the mass residuals of the biofilm did not change when treated with free Ce6 at 4.0 µg/mL compared to that treated with PBS. When light irradiation was applied, the mass residual was reduced by approximately 18%. Treatments with UCONs or Lipo/UCONs at a concentration of 32 µg/mL caused approximately 29% reduction in biofilm mass residuals, no matter with or without irradiation. The dispersal percentage of the biofilm treated with Ce6@Lipo/UCONs was around 28% in dark, similar to that of UCONs, while the treatment under light irradiation caused around 83% reduction of the biofilm mass residuals. The morphology of biofilms under different treatments was evaluated by SEM observation (Figure 5c). Prior to the treatment, the biofilms showed extensive bacterial aggregates and adhesion of extracellular polymeric substances (EPS), with the bacteria exhibiting typical coccus morphology. The biofilms could be moderately disrupted upon the treatments with free Ce6+NIR and UCONs, while the most significant elimination of biofilm mass was observed by the treatment of Ce6@Lipo/UCONs under irradiation, and the aggregated bacterial cells were completely removed. Taken together, Ce6@Lipo/UCONs demonstrated efficient penetration ability into MRSA biofilms and exhibited great bactericidal ability through a synergistic effect between photodynamic inactivation and metal sterilization.

The effect of Ce6@Lipo/UCONs on ROS production in biofilms was investigated (Figure 5d). The biofilm incubated with Ce6@Lipo/UCONs and subjected to laser irradiation exhibited the strongest green fluorescence of ROS among the tested formulations. The abundance of ROS in the biofilm was effective in killing bacteria. In contrast, the group treated with free Ce6 under laser irradiation showed very low or negligible green fluorescence of ROS due to the inability of free Ce6 to penetrate into the biofilm. The fluorescence of ROS in the biofilms treated with UCONs and Lipo/UCONs was also very weak due to their limited bactericidal activities at the tested concentration.

Our findings suggest that Ce6@Lipo/UCONs exhibit a synergistic effect in the ablation of biofilms, which can be attributed to two mechanisms. First, UCONs can effectively kill bacterial cells by the release of metal ions, and at the same time, UCONs can lead to the accumulation of ROS, resulting in irreversible bacterial cell damage. Second, in combination with PDT in chemodynamic therapies, UCONs exhibit enhanced bactericidal efficacy in the treatment of drug-resistant pathogens. However, it is important to note that in vitro methods have their limitations, as they do not precisely mimic the complex in vivo conditions of bacterial environments.



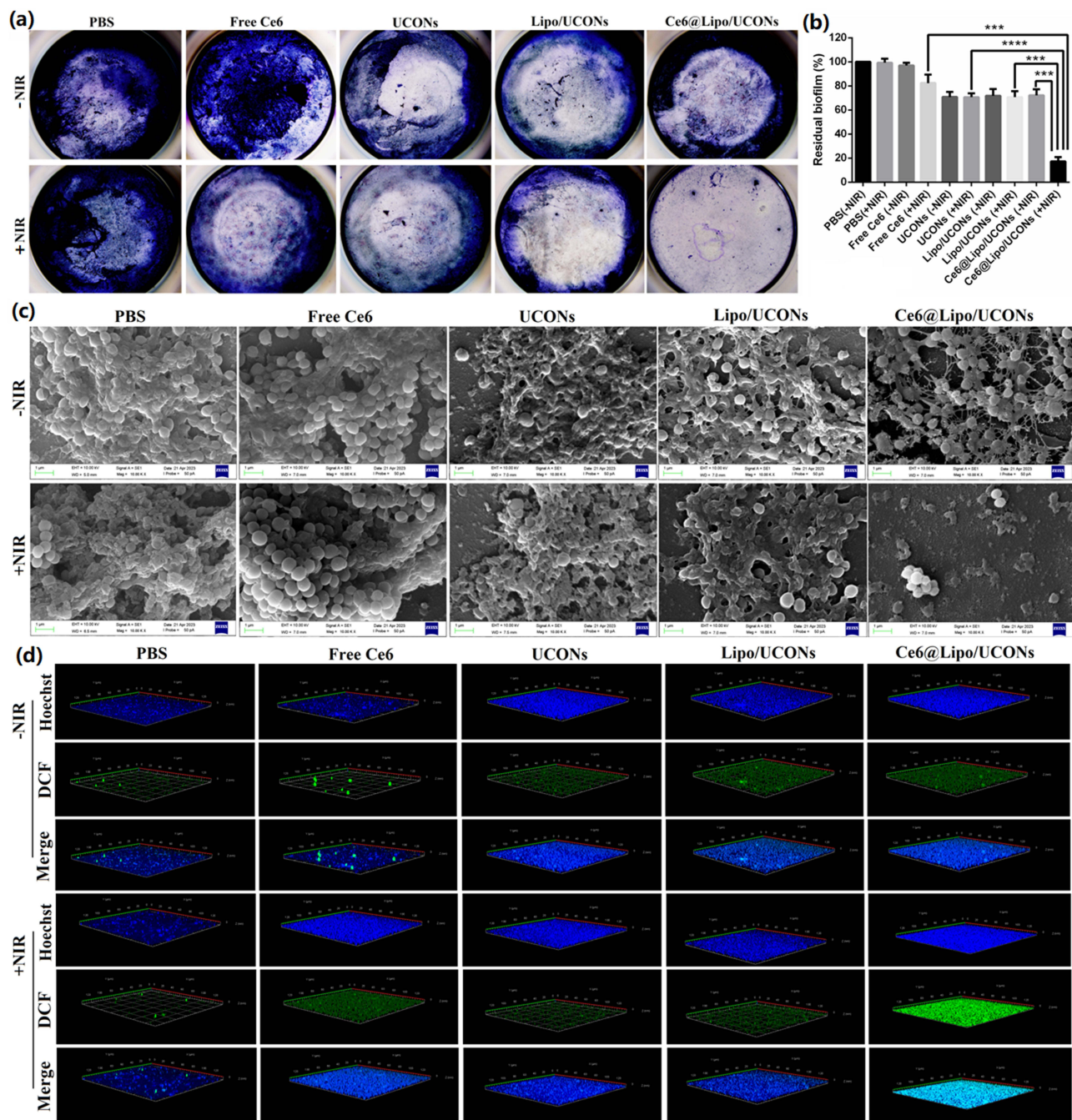


**Figure 5** (a) Biofilm imaging using crystal violet staining, (b) percentages of residual biofilms, (c) residual biofilm imaging using SEM and (d) ROS generation after being treated with PBS, free Ce6, UCONs, Lipo/UCONs and Ce6@Lipo/UCONs overnight. Data are shown as mean  $\pm$  S.D (n = 3), \*\*\*P < 0.001, \*\*\*\*P < 0.0001.

## In vivo Antibacterial Activity

The effectiveness of Ce6@Lipo/UCONs against bacteria in vivo was investigated using a BALB/c mouse model with back abscesses. The experimental design and treatment protocol are shown in Figure 6a. As depicted in Figure 6b, the treatment by Ce6@Lipo/UCONs caused a significant decrease in bacterial counts by approximately 98.3%, which was significantly better than that by Ce6+light. Moreover, UCONs, UCONs+Light, Lipo/UCONs, Lipo/UCONs+Light and Ce6@Lipo/UCONs-treated groups also demonstrated antibacterial activity to some extent by reducing bacterial viabilities to 33.80%, 35.19%, 34.26%, 39.81% and 32.87%, respectively. The body weight of Ce6@Lipo/UCONs-treated BALB/c mice completely recovered to the normal range, indicating that Ce6@Lipo/UCONs exhibited great therapeutic



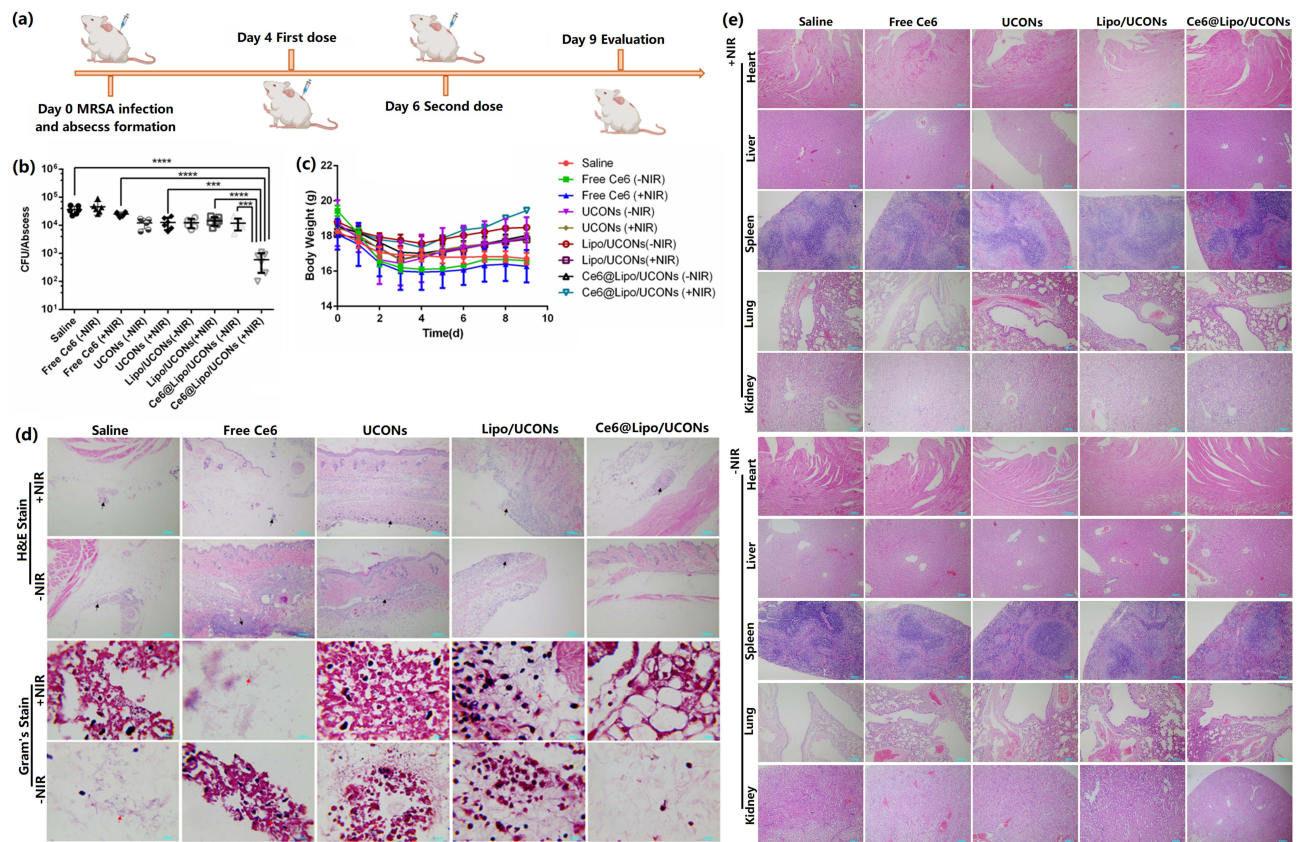


**Figure 6** (a) The experimental design and treatment protocol for MRSA-abscess mice model. (b) Quantitative analysis of the bacteria in the infected tissue, (c) changes in body weight, (d) histological analysis of the infected tissues after H&E staining and Gram's staining, and (e) the major organs after H&E staining. The mice were treated with different formulations (PBS, free Ce6, UCONs, Lipo/UCONs and Ce6@Lipo/UCONs with and without irradiation). Data are shown as mean  $\pm$  S.D (n = 6), \*\*\*P <0.001, \*\*\*\*P <0.0001.

efficiency (Figure 6c). It should be noted that the weight of the mice may be affected by the inflammation and pain caused by the treatments. The antibacterial efficacy of Ce6@Lipo/UCONs was further confirmed through H&E staining and Gram's staining. The saline-treated group exhibited severe subcutaneous tissue necrosis and a high number of bacteria was observed (Figure 6d). On the contrary, the Ce6@Lipo/UCONs-treated group exhibited no obvious abnormality in the subcutaneous tissues, and bacteria could not be detected. Furthermore, Ce6@Lipo/UCONs showed good biocompatibility as no significant pathological changes were observed in the main organs (Figure 6e).

## Conclusions

In this study, a new type of photodynamic cationic ultrasmall copper oxide nanoparticles-loaded liposomes were successfully developed for the treatment of antibiotic-resistant biofilms. These Lipo/UCONs were found to be biocompatible with mammalian cells, and the anionic photosensitizer, Ce6, could be efficiently loaded via electrostatic binding and maintain its photodynamic activity. Ce6@Lipo/UCONs showed improved antibacterial activity not only against planktonic MRSA due to the enhanced bacteria association, but also against mature MRSA biofilm by effective penetration inside the biofilm. Our results demonstrated that the treatment of MRSA biofilms *in vitro* by Ce6@Lipo/UCONs led to significant reduction of biomass and viable pathogens within biofilms. *In vivo* studies were further conducted using a MRSA-abscess mouse model treated with Ce6@Lipo/UCONs and light irradiation. The results show that no obvious abnormality was observed in the subcutaneous tissues and bacteria could not be detected. Histological analysis demonstrates that Ce6@Lipo/UCONs exhibited good biocompatibility as no significant pathological changes were observed in the main organs. In summary, Ce6@Lipo/UCONs developed in this study exhibit high anti-bacterial

activities against both planktonic MRSA and its biofilm through a synergistic effect of metal sterilization and photo-dynamic inactivation, providing a promising approach in the treatment of antibiotic-resistant bacteria.

## Ethics Approval and Consent to Participate

The animal studies were conducted with approval from Institutional Animal Care and Use Committee of Binzhou Medical University. All procedures were performed in accordance with the Chinese National Laboratory Animal-Guideline for Ethical Review of Animal Welfare (GB/T 35892-2018).

## Acknowledgments

The authors thank for the support of Longle Wang (Binzhou Medical University) in data analysis.

## Funding

This study was financially supported by the Taishan Scholar Project of Shandong Province (no. tsqn201909143), and Key Program of Natural Science Foundation of Shandong Province (No. ZR2020KE015).

## Disclosure

The authors report no conflicts of interest in this work.

## References

1. Privalsky TM, Soohoo AM, Wang J, et al. Prospects for antibacterial discovery and development. *J Am Chem Soc.* 2021;143(50):21127–21142. doi:10.1021/jacs.1c10200
2. Blair JM, Webber MA, Baylay AJ, Ogbolu DO, Piddock LJ. Molecular mechanisms of antibiotic resistance. *Nat Rev Microbiol.* 2015;13(1):42–51. doi:10.1038/nrmicro3380
3. Kavcic B, Tkacik G, Bollenbach T. Mechanisms of drug interactions between translation-inhibiting antibiotics. *Nat Commun.* 2020;11(1):4013. doi:10.1038/s41467-020-17734-z
4. Cheng DB, Zhang XH, Gao YJ, et al. Endogenous reactive oxygen species-triggered morphology transformation for enhanced cooperative interaction with mitochondria. *J Am Chem Soc.* 2019;141(18):7235–7239. doi:10.1021/jacs.8b07727
5. Zhu HP, Li B, Liu XM, et al. Interfacial Mo, w-conjugated polarization, and oxygen vacancies of MoO<sub>2</sub>/WO<sub>3</sub> in enhanced microwave therapy for MRSA-induced osteomyelitis. *ACS Nano.* 2022;16(12):21098–21110. doi:10.1021/acsnano.2c09036
6. Qian YX, Deng S, Cong ZH, et al. Secondary amine pendant  $\beta$ -peptide polymers displaying potent antibacterial activity and promising therapeutic potential in treating MRSA-induced wound infections and keratitis. *J Am Chem Soc.* 2022;144(4):1690–1699. doi:10.1021/jacs.1c10659
7. Hu YY, Zhou H, Huang JX, et al. 2-Hydroxypropyl group linked derivatives of indole azoles as potential multifunctional antibacterial candidates for effectively inhibiting the activity of MRSA and responding inflammatory factors. *Chem Asian J.* 2023;18(7):202300054. doi:10.1002/asia.202300054
8. Abee T, Kovacs AT, Kuipers OP, van der Veen S. Biofilm formation and dispersal in gram-positive bacteria. *Curr Opin Biotechnol.* 2011;22:172–179. doi:10.1016/j.copbio.2010.10.016
9. Nassar O, Desouky SE, El-Sherbeiny GM, Abu-Elghait M. Correlation between phenotypic virulence traits and antibiotic resistance in *Pseudomonas aeruginosa* clinical isolates. *Microb Pathog.* 2022;162:105339. doi:10.1016/j.micpath.2021.105339
10. Bjarnsholt T. The role of bacterial biofilms in chronic infections. *APMIS Suppl.* 2013;121:1–58. doi:10.1111/apm.12099
11. Trautner BW, Darouiche RO. Role of biofilm in catheter-associated urinary tract infection. *Am J Infect Control.* 2004;32(3):177–183. doi:10.1016/j.ajic.2003.08.005
12. Song Z, Borgwardt L, Hoiby N, Wu H, Sorensen TS, Borgwardt A. Prosthesis infections after orthopedic joint replacement: the possible role of bacterial biofilms. *Orthop Rev.* 2013;5(2):65–71.
13. Liao Y, Li B, Zhao Z, et al. Targeted theranostics for tuberculosis: a rifampicin-loaded aggregation-induced emission carrier for granulomas tracking and anti-infection. *ACS Nano.* 2020;14(7):8046–8058. doi:10.1021/acsnano.0c00586
14. Abdelhameed RM, Abu-Elghait M, El-Shahat M. Engineering titanium-organic framework decorated silver molybdate and silver vanadate as antimicrobial, anticancer agents, and photo-induced hydroxylation reactions. *J Photoch Photobiol A.* 2022;423:113572. doi:10.1016/j.jphotochem.2021.113572
15. Lan M, Zhao S, Liu W, Lee CS, Zhang W, Wang P. Photosensitizers for photodynamic therapy. *Adv Healthc Mater.* 2019;8(13):e1900132. doi:10.1002/adhm.201900132
16. Abdelhameed RM, Abu-Elghait M, El-Shahat M. Hybrid three MOFs composites (ZIF-67@ZIF-8@MIL-125-NH<sub>2</sub>): enhancement the biological and visible-light photocatalytic activity. *J Environ Eng.* 2020;8(5):104107.
17. Xing XQ, Ma WS, Zhao XY, et al. Interaction between surface charge-modified gold nanoparticles and phospholipid membranes. *Langmuir.* 2018;34(42):12583–12589. doi:10.1021/acs.langmuir.8b01700
18. Jean-François F, Castano S, Desbat B, et al. Aggregation of cateslytin  $\beta$ -sheets on negatively charged lipids promotes rigid membrane domains. A new mode of action for antimicrobial peptides? *Biochemistry.* 2008;47(24):6394–6402. doi:10.1021/bi800448h
19. Lei Y, Tang L, Xie Y, et al. Gold nanoclusters-assisted delivery of NGF siRNA for effective treatment of pancreatic cancer. *Nat Commun.* 2017;8:15130. doi:10.1038/ncomms15130

20. Zhao Y, Tian Y, Cui Y, Liu W, Ma W, Jiang X. Small molecule-capped gold nanoparticles as potent antibacterial agents that target Gram-negative bacteria. *J Am Chem Soc.* 2010;132(35):12349–12356. doi:10.1021/ja1028843
21. Tang H, Zhao X, Jiang X. Synthetic multi-layer nanoparticles for CRISPR-Cas9 genome editing. *Adv Drug Deliv Rev.* 2021;168:55–78. doi:10.1016/j.addr.2020.03.001
22. Luo Z, Zheng K, Xie J. Engineering ultrasmall water-soluble gold and silver nanoclusters for biomedical applications. *Chem Commun.* 2014;50(40):5143–5155. doi:10.1039/C3CC47512C
23. Han B, Wang E. DNA-templated fluorescent silver nanoclusters. *Anal Bioanal Chem.* 2012;402(1):129–138. doi:10.1007/s00216-011-5307-6
24. Song XR, Goswami N, Yang HH, Xie JP. Functionalization of metal nanoclusters for biomedical applications. *Analyst.* 2016;141(11):3126–3140. doi:10.1039/C6AN00773B
25. Javadhesaria SM, Alipourb S, Mohammadnejadc S, Akbarpourc MR. Antibacterial activity of ultra-small copper oxide (II) nanoparticles synthesized by mechanochemical processing against *S. aureus* and *E. coli*. *Mater Sci Eng C.* 2019;105:110011. doi:10.1016/j.msec.2019.110011
26. Jadhav S, Gaikwad S, Nimse M, Rajbhoj A. Copper oxide nanoparticles: synthesis, characterization and their antibacterial activity. *J Clust Sci.* 2011;22:121–129. doi:10.1007/s10876-011-0349-7
27. Liu Y, He L, Mustapha A, Li H, Hu Z, Lin M. Antibacterial activities of zinc oxide nanoparticles against *Escherichia coli* O157:H7. *J Appl Microbiol.* 2009;107(4):1193–1201. doi:10.1111/j.1365-2672.2009.04303.x
28. Baker C, Pradhan A, Pakstis L, Pochan DJ, Shah SI. Synthesis and antibacterial properties of silver nanoparticles. *J Nanosci Nanotechnol.* 2005;5(2):244–249. doi:10.1166/jnn.2005.034
29. Yousef A, Abu-Elghait M, Barghoth MG, Elazzazy AM, Desouky SE. Fighting multidrug-resistant *Enterococcus faecalis* via interfering with virulence factors using green synthesized nanoparticles. *Microb Pathog.* 2022;173(Pt A):105842. doi:10.1016/j.micpath.2022.105842
30. Drulis-Kawa Z, Dorotkiewicz-Jach A. Liposomes as delivery systems for antibiotics. *Int J Pharm.* 2010;387(1–2):187–198. doi:10.1016/j.ijpharm.2009.11.033
31. Goldmann O, Cern A, Muesken M, et al. Liposomal mupirocin holds promise for systemic treatment of invasive *Staphylococcus aureus* infections. *J Control Release.* 2019;316:292–301. doi:10.1016/j.jconrel.2019.11.007
32. Mugabe C, Halwani M, Azghani AO, Lafrenie RM, Omri A. Mechanism of enhanced activity of liposome-entrapped aminoglycosides against resistant strains of *Pseudomonas aeruginosa*. *Antimicrob Agents Chemother.* 2006;50:2016–2022. doi:10.1128/AAC.01547-05
33. Omri A, Suntres ZE, Shek PN. Enhanced activity of liposomal polymyxin B against *Pseudomonas aeruginosa* in a rat model of lung infection. *Biochem Pharmacol.* 2002;64(9):1407–1413. doi:10.1016/S0006-2952(02)01346-1
34. Flemming HC, Wingender J, Szewzyk U, Steinberg P, Rice SA, Kjelleberg S. Biofilms: an emergent form of bacterial life. *Nat Rev Microbiol.* 2016;14:563–575. doi:10.1038/nrmicro.2016.94
35. Hu DF, Y Y, Deng FJ, Jin Q, Ji J. Surface charge switchable supramolecular nanocarriers for nitric oxide synergistic photodynamic eradication of biofilms. *ACS Nano.* 2020;14:347–359. doi:10.1021/acsnano.9b05493
36. Chen XJ, Li W, Jiang X, et al. Hydrogen peroxide-activated nitric oxide-releasing vancomycin-loaded electrostatic complexation for efficient elimination of methicillin-resistant *staphylococcus aureus* abscesses. *Mol Pharm.* 2023;20(1):711–721. doi:10.1021/acs.molpharmaceut.2c00888

International Journal of Nanomedicine

Dovepress

## Publish your work in this journal

The International Journal of Nanomedicine is an international, peer-reviewed journal focusing on the application of nanotechnology in diagnostics, therapeutics, and drug delivery systems throughout the biomedical field. This journal is indexed on PubMed Central, MedLine, CAS, SciSearch®, Current Contents®/Clinical Medicine, Journal Citation Reports/Science Edition, EMBase, Scopus and the Elsevier Bibliographic databases. The manuscript management system is completely online and includes a very quick and fair peer-review system, which is all easy to use. Visit <http://www.dovepress.com/testimonials.php> to read real quotes from published authors.

Submit your manuscript here: <https://www.dovepress.com/international-journal-of-nanomedicine-journal>